JOURNAL OF GEOPHYSICAL RESEARCH, VOL. 112, D08204, doi:10.1029/2006JD007533, 2007

Click Here for Full Article

Polar mesospheric cloud mass and the ice budget: 1. Quantitative interpretation of mid-UV cloud brightness observations

Christoph R. Englert[1] and Michael H. Stevens[1]

Received 19 May 2006; revised 23 October 2006; accepted 1 January 2007; published 20 April 2007.

[1] We investigate the retrieval of column ice mass from mid-UV solar scattering polar mesospheric cloud (PMC) observations to help constrain estimates of the ice budget of the polar summer mesosphere. First, we show that the backscattered brightness from PMC particles is roughly proportional to the mass of the ice particles. Second, we quantify the sensitivity of the retrieved PMC column ice mass to the particle size distribution for a viewing geometry typical for a subset of Solar Backscattered UltraViolet (SBUV) satellite data taken at 70 ± 2.5°N. Considering a wide range of Gaussian size distributions using spherical particles with peak radii between 15 nm and 100 nm and widths between 10 nm and 20 nm, we find that we can constrain the inferred ice column mass to ±43% for 95% of the distributions in this range. For this scenario we also show that spheroids with axis ratios of 0.5, 2.0 and 5.0 generally decrease the sensitivity of the inferred ice column mass to the size distribution. Third, we quantify the sensitivity of the retrieved PMC column ice mass for a viewing geometry typical for a subset of Student Nitric Oxide Explorer (SNOE) satellite data. Using the same wide range of size distributions, we show that the inferred ice column mass can be constrained to ±33% for 95% of the distributions in this range. The results of this paper are used by two companion papers to investigate the polar mesospheric ice budget.

Citation: Englert, C. R., and M. H. Stevens (2007), Polar mesospheric cloud mass and the ice budget: 1. Quantitative interpretation of mid-UV cloud brightness observations, *J. Geophys. Res.*, *112*, D08204, doi:10.1029/2006JD007533.

1. Introduction

[2] Observations of polar mesospheric clouds (PMCs) from space are typically made by instruments designed to measure other properties of the mesosphere and lower thermosphere. Therefore the observation techniques, sensitivities, geographical and temporal coverage, and spatial resolution vary widely for the different instruments. Examples are visible and infrared (IR) solar occultation measurements [*Hervig et al.*, 2001; *Eremenko et al.*, 2005; *Debrestian et al.*, 1997], ultraviolet (UV) nadir viewing albedo measurements [*DeLand et al.*, 2003, 2006a], or UV limb viewing solar scattering observations [e.g., *Carbary et al.*, 2003; *von Savigny et al.*, 2005; *Bailey et al.*, 2005].

[3] Typically, results from PMC investigations are reported using data from a single instrument. They provide insight on cloud properties like altitude, occurrence frequency, particle size, and particle composition. Because of the highly variable nature of PMCs and because of instrument specific differences like sensitivity, viewing geometry or lighting conditions, it can be difficult to place these results in the context of each other and in the context of model results.

[4] As more measurements become available and PMC microphysical model calculations improve [*Rapp and Thomas*, 2006; *Berger and Lübken*, 2006; *Siskind et al.*, 2007], it is of increasing importance to compare individual data sets with each other and with model calculations in a quantitative way.

[5] We herein focus on a method of comparison using a measure of how much ice is present in a given PMC observation: The vertical column ice mass. This quantity has been derived using model results [*Turco et al.*, 1982; *Jensen and Thomas*, 1988; *Rapp and Thomas*, 2006] and using observations from the Solar Mesosphere Explorer (SME) [*Thomas*, 1984; *Thomas and McKay*, 1985]. More recently, *Stevens et al.* [2005] derived the column ice mass using one season of PMC albedo observations from the Solar Backscattered UltraViolet (SBUV) instrument and found general agreement with the SME value.

[6] This work has three major objectives. First, we show that the column ice mass, when derived from mid-UV observations of backscattered ($\theta > 90°$) sunlight, is relatively insensitive to characteristics of the particle size distribution (mean radius and width) and the particle shape. Second, we determine the relation between the 252 nm PMC albedo measured by SBUV and the column ice mass for a typical scattering angle, assuming a wide range of particle size distributions. Third, we quantify the sensitivity of column ice mass to PMC limb radiance measurements at 215 nm for

[1]Space Science Division, Naval Research Laboratory, Washington, D. C., USA.

This paper is not subject to U.S. copyright. Published in 2007 by the American Geophysical Union.
0148-0227/07/2006JD007533$09.00

a typical scattering angle of measurements by the Student Nitric Oxide Explorer (SNOE). All of these objectives will lay the foundation for the companion paper by *Stevens et al.* [2007], who also include the cloud frequency to compare the total PMC ice mass observed by SBUV and SNOE.

2. Inferring Column Ice Mass From Mid-UV Scattering Observations

[7] In this work we consider measurement scenarios typical for mid-UV observations of SBUV and SNOE. We include the instrument name whenever a property is a function of the sensitivity or viewing geometry of the instrument. For example, we will use "SNOE PMC column ice mass" to indicate that it is a property derived from data of a particular instrument and is therefore subject to its observational parameters. We introduce this nomenclature because even if two instruments look at the same cloud field, the derived PMC quantity can be different because of different instrument sensitivity or viewing geometry.

[8] Inferring the vertical column ice mass from mid-UV scattering signals requires the field of view geometry, the observed wavelength band, and the scattering angle, all of which are known for the satellite observations herein. However, it also depends on less well known parameters, namely the cloud temporal and spatial variations, cloud particle shape, the complex index of refraction of ice around 140 K, and the particle size distribution relevant to the observations. These are discussed in the context of our analysis below.

2.1. Cloud Variations

[9] Ground based observations of PMCs or noctilucent clouds (NLCs) show that they have a complex morphology on scales down to about ~10 km or less and evolve on timescales of tens of minutes [*Witt*, 1962; *Gadsden*, 1982; *Taylor et al.*, 2002]. Satellite observations, however, currently do not resolve these fine spatial structures, nor do they completely sample the entire PMC region at all times, so that we have to make simplified assumptions to infer the PMC column ice mass. In this work, we assume that the spatial sampling of the cloud region under investigation (170 km^2 nadir footprint for each SBUV measurement) is dense enough to be representative. For limb observations, we assume a spherical symmetry of the cloud layer and a cloud thickness of 1 km (see section 4.1).

2.2. Cloud Particle Shape

[10] Most previous analyses of PMC optical properties have assumed spherical particles with a lognormal size distribution [e.g., *Rusch et al.*, 1991; *von Cossart et al.*, 1999; *Stevens et al.*, 2005; *von Savigny et al.*, 2005; *DeLand et al.*, 2006b]. However, evidence of nonsphericity has been presented using satellite observations in the infrared [*Eremenko et al.*, 2005] and ground based lidar observations [*Baumgarten et al.*, 2002]. The lidar depolarization measurements show nonspherical particles with axis ratios (AR) between 2.5 and 10. However, the authors point out that the depolarization part of the PMC is located about 1 km higher than the altitude of the maximum backscattering suggesting that the large axis ratios are predominantly present in the initial growth phase of the particles. *Rapp et al.* [2007] argue that the interpretation of mid-UV PMC observations requires consideration of nonspherical particles if the ice particles are represented by a Gaussian size distribution as suggested by microphysical models [*Berger and von Zahn*, 2002; *Rapp and Thomas*, 2006].

[11] We will use a Gaussian size distribution and also consider the implications of nonspherical particles for the SBUV observations. We consider spherical particles as well as spheroids with axis ratios of 5.0, 2.0 (oblate) and 0.5 (prolate). For the analysis of the SNOE data we only consider spherical particles.

2.3. Index of Refraction

[12] The complex index of refraction of ice in the mid-UV at PMC temperatures has never been measured. The best available estimate for the wavelength-dependent refractive index is provided by *Warren* [1984] who compiled measurements of the imaginary part over most relevant portions of the electromagnetic spectrum and used the Kramers-Kronig relation to calculate the real part. The tabulated values are recommended for use between 213.15 K and 273.15 K. In the wavelength region of interest here, the imaginary part is many orders of magnitude smaller than the real part (see Table 1). *Warren* [1984] points out that while the real part can be obtained reliably the imaginary part cannot. However, since the imaginary part is so small, our results are not sensitive to its uncertainty [*Perovich and Govoni*, 1991]. In this work, we will use the data published by *Warren* [1984] and perform an interpolation to obtain the refractive indices at the relevant wavelengths.

2.4. Particle Size Distribution

[13] When the PMC column ice mass (η_{ice}) is inferred from mid-UV PMC radiance or albedo measurements, its dependence on the particle size distribution can be written as follows, under the assumption of an optically thin cloud:

$$\begin{aligned}\eta_{ice} &= \frac{4\pi}{3}\rho_{ice}\frac{L_{\theta,\lambda}}{\Phi_\lambda}\frac{\int n(r)r^3dr}{\int n(r)\sigma(\theta,\lambda,r)dr}\\ &= \frac{4\pi}{3}\rho_{ice}A_{\theta,\lambda}\frac{\int n(r)r^3dr}{\int n(r)\sigma(\theta,\lambda,r)dr}\end{aligned} \quad (1)$$

where ρ_{ice} is the water ice density, $L_{\theta,\lambda}$ is the measured radiance at the scattering angle θ and wavelength λ, Φ_λ is the solar flux, n(r) is the radius-dependent normalized number density of the PMC particles, $\sigma(\theta, \lambda, r)$ is the differential scattering cross section, and $A_{\theta,\lambda}$ is the albedo.

[14] Equation (1) shows that the retrieved ice column mass is independent of the particle size distribution, in case the differential cross section is proportional to r^3. In this case, no knowledge of the particle size distribution would be necessary to retrieve the ice column mass in the instruments field of view. We therefore have to take a closer look at the particle radius dependence of $\sigma(\theta, \lambda, r)$:

[15] Under forward scattering conditions, the differential cross section of PMC particles in the mid-UV exhibits a dependence on radius similar to Rayleigh scattering [e.g., *Rapp and Thomas*, 2006]. Thus, for forward scattering angles ($\theta < 90°$), $\sigma(\theta, \lambda, r)$ is roughly proportional to the sixth power of the particle radius. This geometry is typical of SNOE PMC observations in the Southern Hemisphere.

Table 1. Input Parameters for Ice Mass Calculations

Input Parameter	Value
Wavelength	252.0 nm (SBUV), 215.0 nm (SNOE)
Scattering angle	131° (SBUV), 139° (SBUV)
Particle shape	spherical
Particle size distribution	truncated Gaussian
Ice density[a]	932 kg/m^3
Ice refractive index[b]	1.3498 + 8.445·10^{-9} i (SBUV, 252 nm), 1.3744 + 1.248·10^{-8} i (SNOE, 215 nm)
Solar flux[c]	37.5 mW/m^2/nm (SNOE, 215 nm channel)

[a]*Gadsden* [1998].
[b]Interpolation of data published by *Warren* [1984].
[c]*Woods et al.* [1996].

Figure 1a shows the differential scattering cross section versus radius for a monodisperse ice particle distribution in a forward scattering geometry, clearly illustrating the r^6 dependence for particles with r < 80 nm. For typical Gaussian or lognormal size distributions this r^6 dependence does not change significantly, so that we expect the retrieved column mass η_{ice} to be strongly dependent on the assumed size distribution. For example, assuming $\sigma(\theta, \lambda, r)$ is proportional to r^6 the column ice mass in equation (1) would be proportional to r^{-3} for a given albedo and a monodisperse size distribution. Previously reported cloud particle sizes typically vary between about 15 and 100 nm [e.g., *Thomas*, 1984; *Thomas and McKay*, 1985; *Rusch et al.*, 1991; *Debrestian et al.*, 1997; *von Cossart et al.*, 1999; *Carbary et al.*, 2002; *von Savigny et al.*, 2005; *Karlsson and Rapp*, 2006]. This uncertainty in the radius would result in a factor of about 300 in the retrieved mass under the conditions specified in Figure 1a. A reasonable determination of the column ice mass would be very difficult in this Rayleigh like regime.

[16] However, the r^6 dependence of the differential scattering cross section does not hold under all observation conditions in the mid-UV. For backscattering angles (θ > 90°), the mid-UV differential scattering cross sections calculated using standard Mie theory [*Bohren and Huffman*, 1983] have a much weaker radius dependence. Figure 1b shows the scattering cross section for one typical SBUV wavelength (252.0 nm) and scattering angle (131°). The three solid curves represent a monodisperse distribution (black) as well as a lognormal particle size distribution (blue) and a truncated Gaussian distribution (red). The truncated Gaussian distribution is defined as follows [*Berger and von Zahn*, 2002]:

$$n(r) = \frac{C}{\sqrt{2\pi}\sigma_G} \exp\left(-\frac{(r-r_0)^2}{2\sigma_G^2}\right), \quad r > 0 \text{ nm} \tag{2}$$

$$\int_{0nm}^{\infty} n(r)dr = 1 \tag{3}$$

where r_0 is the peak radius, σ_G is the width of the distribution and C is a normalization factor. Figure 1b illustrates that for monodisperse particles larger than about 30 nm, and particle size distributions (Gaussian or lognormal) with peak radii larger than about 30 nm, the scattering cross section dependence is much closer to r^3 (dashed green line) than r^6 (dotted green line). Consideration of randomly oriented nonspherical particles yields similar results for which the resonances in the differential cross section, like the one around 80 nm in Figure 1b, are even weaker.

[17] This analysis of mid-UV scattering properties of PMCs has two important implications. First, the mid-UV PMC observations will be more sensitive to large particles in a forward scattering geometry (Figure 1a). Second, the differential cross section of cloud particles is roughly proportional to the particle volume or mass for a backward scattering geometry (Figure 1b). This second implication allows us to retrieve the PMC column ice mass from backscattered solar UV data with only limited knowledge of the particle size distribution.

[18] In the following we are going to consider a very wide range of truncated Gaussian distributions with 15 nm < r_0 < 100 nm and 10 nm < σ_G < 20 nm. This distribution range

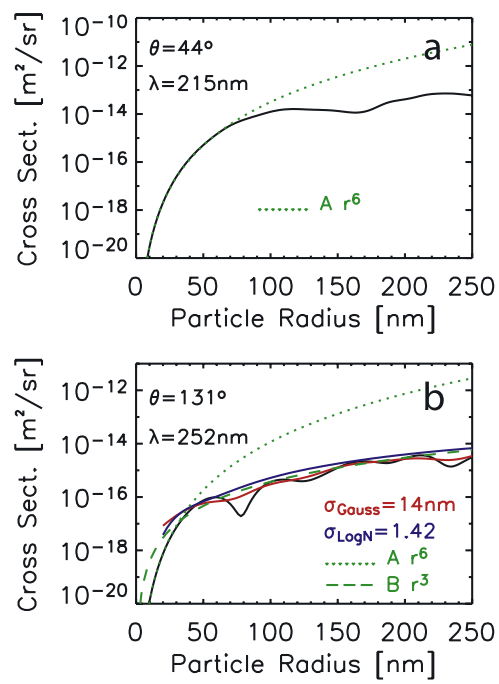

Figure 1. (a) Example of a forward scattering differential cross section versus particle radius. The wavelength and scattering angle indicated are relevant to typical SNOE PMC observations in the Southern Hemisphere [*Bailey et al.*, 2005]. The calculation assumes spherical water ice particles and shows an r^6 dependence for typical PMC particle radii (r < 80 nm). (b) Example of a backward scattering cross section versus particle radius. The wavelength and scattering angle are typical for SBUV observations near 70°N [*Stevens et al.*, 2007] assuming a monodisperse distribution (black), a lognormal particle size distribution (blue), and a truncated Gaussian distribution (red). The scale factors A and B of the r^6 than r^3 dependencies (green) are chosen to represent the model calculations for small and large radii, respectively. For monodisperse particles larger than about 30 nm, as well as particle size distributions with median radii larger than about 30 nm and typical distribution widths [*von Cossart et al.*, 1999; *Rapp and Thomas*, 2006], the scattering cross section dependence is much closer to r^3 than r^6.

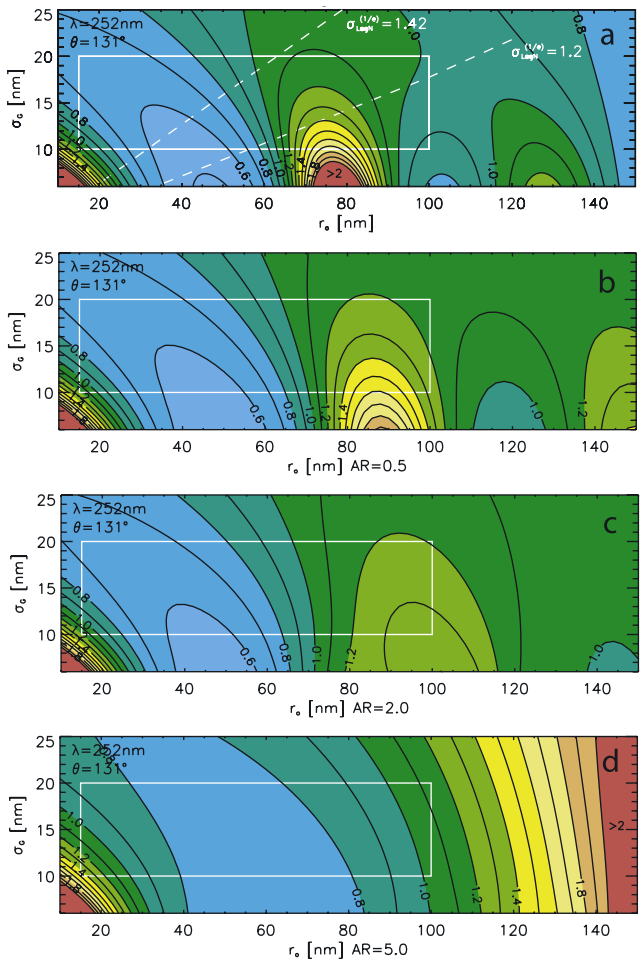

Figure 2. (a) Relative change in retrieved column ice mass as a function of r_0 and σ_G for the 252 nm SBUV wavelength cannel, a scattering angle of 131°, and spherical particles. The white rectangle represents the area of the considered PMC particle radii and Gaussian distribution widths. The two dashed white lines represent size distributions that have the same 1/e width as lognormal distributions with a width parameter of 1.2 and 1.42, respectively. (b) Same as Figure 2a but for randomly oriented prolate spheroids with an AR of 0.5. (c) Same as Figure 2a but for randomly oriented oblate spheroids with an AR of 2. (d) Same as Figure 2a but for randomly oriented oblate spheroids with an AR of 5. Contours of all panels are normalized to the result for spherical particles at r_0 = 60 nm and σ_G = 15 nm so that they can be compared directly.

includes practically all characteristic radii that have recently been inferred from PMC measurements [*Thomas*, 1984; *Thomas and McKay*, 1985; *Rusch et al.*, 1991; *Debrestian et al.*, 1997; *von Cossart et al.*, 1999; *Carbary et al.*, 2002; *von Savigny et al.*, 2005; *Karlsson and Rapp*, 2006]. It also covers the r_0 and σ_G resultant of most scenarios in a model study by *Rapp and Thomas* [2006].

3. PMC Mass Column: Nadir Viewing

3.1. SBUV Viewing Geometry and Wavelength

[19] SBUV observes PMCs in the nadir using five narrow band spectral channels [*DeLand et al.*, 2003]. In the companion paper by *Stevens et al.* [2007], we use data from the 252.0 nm channel and scattering angles around 131°. Thus we will use these parameters for this study so that the results can be applied directly.

[20] Compared to limb viewing instruments like SNOE, SBUV is significantly less sensitive to PMCs because it views the clouds against the bright mid-UV albedo of the Earth's atmosphere. This background can fluctuate because of stratospheric ozone variations [e.g., *Thomas et al.*, 1991]. As a result, the albedo contrast between a clear air observation and a PMC observation is small and "only the brightest portion of the PMC population" can be identified [*DeLand et al.*, 2006a]. This is of particular importance for the interpretation of the SBUV data, since the result will be representative of only the bright clouds that exceed the SBUV sensitivity threshold.

3.2. SBUV Column Ice Mass Versus Particle Size Distribution and Particle Shape

[21] We will now quantify the change in retrieved SBUV column ice mass for different particle size distributions and particle shapes. Figure 2a shows the relative change in retrieved SBUV column ice mass as a function of r_0 and σ_G calculated for spherical ice particles (AR of 1.0). The relative change is arbitrarily normalized to the result at r_0 = 60 nm and σ_G = 15 nm. As mentioned in section 2, the changes are relatively small (tens of percent) when compared to the changes expected from an r^6 dependence of the scattering cross section. Also shown in Figure 2a are two dashed lines that correspond to Gaussian distributions with the same 1/e widths as lognormal distributions with width parameters of 1.42 and 1.2. These widths correspond to the average and minimum width found by *von Cossart et al.* [1999] in their analysis of ground-based observations.

[22] We also consider how the relative mass varies with the characteristic size and width of nonspherical particles [*Mishchenko and Travis*, 1998]. Figures 2b–2d are similar to Figure 2a, but assume randomly oriented prolate and oblate spheroids with AR of 0.5, 2.0, and 5.0. For the spheroids in Figures 2b–2d, r_0 is defined as the volume equivalent sphere radius. Figures 2a–2d are normalized to the same absolute mass per albedo value, so they can be compared directly. The comparison of Figures 2a–2d shows that the assumption of randomly oriented spheroids does not necessarily increase the uncertainty of the resulting column ice mass. In fact, the results shown here exhibit even less variation of the retrieved mass because of the smaller magnitude of the resonances in the scattering cross sections.

3.3. SBUV Column Ice Mass Versus Observed Albedo

[23] Figure 3 shows the retrieved SBUV vertical column ice mass versus the SBUV PMC albedo at 252.0 nm resulting from standard Mie scattering calculations using spherical particles and a truncated Gaussian size distribution as defined in equations (2) and (3). The shaded area covers the results for 95% of all particle size distributions within the range shown in Figure 2a (15 nm < r_0 < 100 nm and 10 nm < σ_G < 20 nm). The 95% criterion avoids the relatively large positive uncertainty that would result from a few particle size distributions within the unique resonance feature near r_0 = 75 nm and σ_G = 10 nm in Figure 2a. For a typical SBUV PMC albedo of 10^{-5} sr^{-1}, the vertical

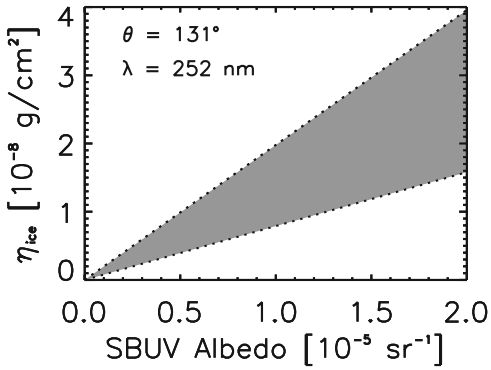

Figure 3. Retrieved SBUV vertical column ice mass versus SBUV PMC albedo at 252 nm assuming spherical particles and a truncated Gaussian size distribution. The shaded area (±43%) represents 95% of all solutions assuming distributions with 15 nm < r_0 < 100 nm and 10 nm < σ_G < 20 nm as shown in Figure 2a.

column ice mass is therefore about 1.47×10^{-8} g/cm^2 (+35%/−46% referenced to r_0 = 60 nm and σ_G = 15 nm). Figure 3 is analogous to results shown by *Stevens et al.* [2005] (their Figure 4) showing the relationship between the 252.0 nm albedo and the SBUV column ice mass. The main differences between these two figures are the distribution shape (Gaussian versus lognormal) and the median particle radius (15–100 nm versus 55 nm). The column ice mass versus albedo shown by *Stevens et al.* [2005] for r = 55 nm, θ = 130°, and σ_{LogN} = 1.42 falls almost exactly in the center of the shaded area in Figure 3, as expected from the calculations shown in Figure 2a. Table 1 summarizes all relevant inputs to the SBUV ice column mass calculations shown in Figure 3.

4. PMC Mass Column: Limb Viewing

[24] In contrast to the SBUV observations, most satellite observations of PMCs are made on the limb. SNOE is one such satellite. We now consider mid-UV observations of backscattered sunlight from PMCs made by SNOE and explore how the column ice mass can be derived from the measured cloud radiances.

4.1. SNOE Viewing Geometry and Wavelengths

[25] SNOE observed PMCs between 1998 and 2003 in both hemispheres up to 82° latitude. For the following calculations, we use a wavelength of 215 nm and a scattering angle of 136° because the results are then directly applicable to data presented in the companion paper by *Stevens et al.* [2007].

[26] SNOE is a spinning satellite whose axis of rotation is roughly perpendicular to the orbit plane and the ultraviolet spectrometer (UVS) points perpendicular to the axis of rotation [*Bailey et al.*, 2005]. Its instantaneous field of view projected on the limb has a height of 3.2 km at the tangent point [*Merkel et al.*, 2001]. The satellite spins with a rate of 5 rpm so that the field of view performs an altitude scan on the limb. Each exposure is 2.4×10^{-3} s long. The constant motion of the uniformly sensitive field of view during the exposure results in an effective field of view with a triangular sensitivity function where the half points of the triangle are separated by about 3.2 km in altitude. This viewing geometry is similar but not identical to the UVS on the Solar Mesosphere Explorer (SME) [*Thomas and McKay*, 1985].

[27] In the SNOE data set, PMCs are identified by the enhanced limb radiance caused by the UV scattering of the ice particles. Since UVS observes the PMCs against a dim background, it is more sensitive than SBUV and can identify many more PMCs than SBUV, as discussed by *Stevens et al.* [2007]. Aside from its higher sensitivity, the most important difference between the column ice mass inferred by SNOE and that inferred from SBUV is that the longer SNOE line of sight through the cloud layer yields a much larger slant column ice mass. We uniformly reduce the observed SNOE slant column ice mass by a single geometrical factor to convert it into vertical column ice mass. This factor has been previously derived for the similar SME experiment by *Thomas and McKay* [1985] assuming a 1 km cloud layer thickness. Using a field-of-view width of 3.2 km and a 1 km thick cloud layer, we find this scale factor to be 97.1 for SNOE. Note that this factor is very insensitive to the assumed cloud thickness. Cloud thicknesses of 2 km and 0.5 km as observed by *Fiedler et al.* [2003] result in scale factor changes of less than 2.2%.

4.2. Particle Size Distribution Relevant to SNOE

[28] As for SBUV, we find the sensitivity of the retrieved SNOE column ice mass considering the wide range of particle size distributions with 15 nm < r_0 < 100 nm and 10 nm < σ_G < 20 nm. Figure 4 shows the relative change in the SNOE PMC column ice mass as a function of r_0 and σ_G with the distribution range outlined in white. The data is normalized to r_0 = 60 nm and σ_G = 15 nm.

4.3. SNOE Column Ice Mass Versus Observed Radiance

[29] Figure 5 shows the retrieved SNOE vertical column ice mass versus the SNOE PMC radiance at 215 nm resulting from standard Mie scattering calculations using spherical particles and a truncated Gaussian size distribution as defined in equations (2) and (3). The shaded area covers the results for 95% of all particle size distributions within the range shown in Figure 4 (15 nm < r_0 < 100 nm and 10 nm < σ_G < 20 nm). For a typical SNOE cloud brightness

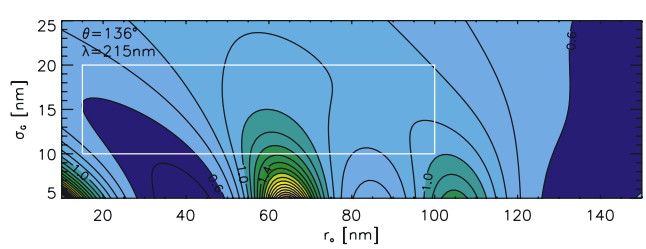

Figure 4. Relative change in retrieved column ice mass as a function of r_0 and σ_G for the 215 nm SNOE channel and a scattering angle of 136°, assuming spherical particles. The white rectangle represents the area of the considered PMC particle radii and Gaussian distribution widths. The contours are normalized to the solution at r_0 = 60 nm and σ_G = 15 nm.

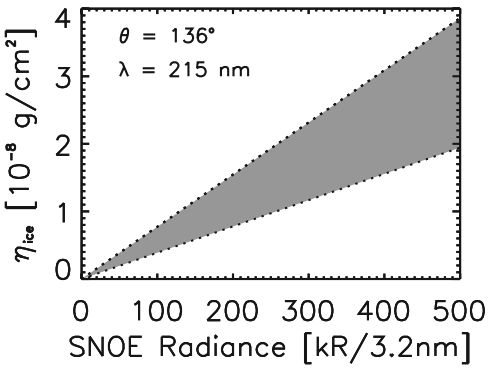

Figure 5. Retrieved SNOE vertical column ice mass versus SNOE PMC spectral radiance at 215 nm assuming spherical particles and a truncated Gaussian size distribution. The shaded area (±33%) represents 95% of all solutions assuming distributions with 15 nm < r_0 < 100 nm and 10 nm < σ_G < 20 nm as shown in Figure 4. The derived slant column ice mass has been scaled by a factor of 97.1 to obtain vertical column ice mass (see text).

of 200 kR/3.2 nm at 215 nm, the vertical column ice mass is $\sim 1.48 \times 10^{-8}$ g/cm^2 (+4%/−48% referenced to r_0 = 60 nm and σ_G = 15 nm) similar to the typical SBUV measurement and consistent with previous analyses using the similar SME data set [*Thomas and McKay*, 1985].

[30] The result that the retrieved vertical column ice masses for typical SNOE and SBUV measurements are similar might seem contradictory to the statement that SNOE is much more sensitive, since one might argue that SNOE measures many more dim clouds with smaller column ice masses. However, we point out that the similarity is the result of the normalization of both retrievals to r_0 = 60 nm and σ_G = 15 nm. Should, for example, the typical particle size for SNOE PMC detections be somewhat smaller than 60 nm, the retrieved typical SNOE column ice mass would decrease as shown in Figure 4. This idea is discussed further in the companion paper by *Stevens et al.* [2007]. Since we do not use any size information determined directly from the individual data sets, we chose to reference the retrieved column ice masses to the same particle size distribution and include any differences in the uncertainties. In case information about the size distributions within the two data sets becomes available, Figures 2 and 4 can be used to determine the column ice mass with less uncertainty.

[31] Table 1 summarizes all relevant inputs to the SNOE column ice mass calculations in Figure 5. *Stevens et al.* [2007] show how the column ice mass can be used together with the cloud occurrence frequency to compare the SNOE and SBUV data sets and to estimate the total mesospheric ice mass.

5. Conclusions

[32] Because of its insensitivity to the ice particle size distribution, the PMC column ice mass is well suited for comparisons between measurements and with microphysical model calculations [*Stevens et al.*, 2007; *Siskind et al.*, 2007]. Generally, the limited information available for the PMC ice particle size distribution results in significant uncertainties when the column ice mass is derived from forward scattered observations of mid-UV sunlight. This is the consequence of the r^6 dependence of the scattering cross section, which applies in these conditions. However, we find that for a typical backscattering geometry ($\theta > 90°$), mid UV (215 nm, 252 nm) scattering cross sections of PMC particles with sizes greater than ~30 nm have a particle radius dependence closer to r^3 than to r^6. This means that the PMC brightness is roughly proportional to the ice volume and thus only weakly dependent on the size distribution of the PMC particles. We find that this conclusion not only applies to spherical cloud particles but also to spheroids with moderate axis ratios (0.5 < AR < 5.0).

[33] We use a wide range of particle size distributions that practically covers all characteristic particle radii inferred from measurements. In particular, we consider truncated Gaussian distributions with 15 nm < r_0 < 100 nm and 10 nm < σ_G < 20 nm as a constraint for inferring the PMC vertical column ice mass. Consideration of 95% of all possible solutions yields a +35%/−46% (referenced to r_0 = 60 nm and σ_G = 15 nm) uncertainty in the PMC column ice mass observed by SBUV. Assuming prolate (oblate) spheroids with an AR of 0.5 (2.0 and 5.0), yields column mass densities within the uncertainty of the spherical particles. For the limb viewer SNOE, the uncertainties in the particle size distribution yield even smaller uncertainties in the vertical column ice mass (+4%/−48%, referenced to r_0 = 60 nm and σ_G = 15 nm).

[34] **Acknowledgments.** This work was supported by the Office of Naval Research (ONR) and NASA. We thank Matthew DeLand (Science Systems and Applications, Inc, MD) and Scott Bailey (Virginia Tech, VA) for many useful discussions on the SBUV and SNOE data. We would also like to thank Michael Mishchenko of NASA for making his T-Matrix code publicly available (http://www.giss.nasa.gov/~crmim/t_matrix.html).

References

Bailey, S. M., A. W. Merkel, G. E. Thomas, and J. N. Carstens (2005), Observations of polar mesospheric clouds by the Student Nitric Oxyde Explorer, *J. Geophys. Res.*, *110*, D13203, doi:10.1029/2004JD005422.

Baumgarten, G., K. H. Fricke, and G. von Cossart (2002), Investigation of the shape of noctilucent cloud particles by polarization lidar technique, *Geophys. Res. Lett.*, *29*(13), 1630, doi:10.1029/2001GL013877.

Berger, U., and F.-J. Lübken (2006), Weather in mesospheric ice layers, *Geophys. Res. Lett.*, *33*, L04806, doi:10.1029/2005GL024841.

Berger, U., and U. von Zahn (2002), Icy particles in the summer mesopause region: Three-dimensional modeling of their environment and two-dimensional modeling of their transport, *J. Geophys. Res.*, *107*(A11), 1366, doi:10.1029/2001JA000316.

Bohren, C. F., and D. R. Huffman (1983), *Absorption and Scattering of Light by Small Particles*, Wiley-Interscience, Hoboken, N. J.

Carbary, J. F., D. Morrison, and G. J. Romick (2002), Particle characteristics from the spectra of polar mesospheric clouds, *J. Geophys. Res.*, *107*(D23), 4686, doi:10.1029/2001JD001154.

Carbary, J. G., D. Morrison, and G. J. Romick (2003), Ultraviolet imaging and spectrographic imaging of polar mesospheric clouds, *Adv. Space Res.*, *31*(9), 2091–2096.

Debrestian, D. J., J. D. Lumpe, R. M. Bevilacqua, E. P. Shettle, J. S. Hornstein, and J. J. Olivero (1997), POAM II observations of polar mesospheric clouds in the Southern Hemisphere, *Adv. Space Res.*, *19*, 587–590.

DeLand, M. T., E. P. Shettle, G. E. Thomas, and J. J. Olivero (2003), Solar Backscattered Ultraviolet (SBUV) observations of polar mesospheric clouds (PMCs) over two solar cycles, *J. Geophys. Res.*, *108*(D8), 8445, doi:10.1029/2002JD002398.

DeLand, M. T., E. P. Shettle, G. E. Thomas, and J. J. Olivero (2006a), A quarter-century of satellite PMC observations, *J. Atmos. Sol. Terr. Phys.*, *68*, 9–29.

DeLand, M. T., E. P. Shettle, G. E. Thomas, and J. J. Olivero (2006b), Spectral measurements of PMCs from SBUV/2 instruments, *J. Atmos. Sol. Terr. Phys.*, *68*, 65–77.

Eremenko, M. N., S. V. Petelina, A. Y. Zasetsky, B. Karlsson, C. P. Rinsland, E. J. Llewellyn, and J. J. Sloan (2005), Shape and composition of PMC particles derived from satellite remote sensing measurements, *Geophys. Res. Lett.*, *32*, L16S06, doi:10.1029/2005GL023013.

Fiedler, J., G. Baumgarten, and G. von Cossart (2003), Noctilucent clouds above ALOMAR between 1997 and 2001: Occurrence and properties, *J. Geophys. Res.*, *108*(D8), 8453, doi:10.1029/2002JD002419.

Gadsden, M. (1982), Noctilucent clouds, *Space Sci. Rev.*, *33*, 279–334.

Gadsden, M. (1998), Noctilucent clouds seen at 60°N: Origin and development, *J. Atmos. Sol. Terr. Phys.*, *60*, 1763–1772.

Hervig, M., et al. (2001), First confirmation that water ice is the primary component of polar mesospheric clouds, *Geophys. Res. Lett.*, *28*(6), 971–974.

Jensen, E., and G. E. Thomas (1988), A growth-sedimentation model of polar mesospheric clouds: Comparison with SME measurements, *J. Geophys. Res.*, *93*, 2461–2473.

Karlsson, B., and M. Rapp (2006), Latitudinal dependence of noctilucent cloud growth, *Geophys. Res. Lett.*, *33*, L11812, doi:10.1029/2006GL025805.

Merkel, A. W., C. A. Barth, and S. M. Bailey (2001), Altitude determination of ultraviolet measurements made by the Student Nitric Oxide Explorer, *J. Geophys. Res.*, *106*(A12), 30,283–30,290.

Mishchenko, M. I., and L. D. Travis (1998), Capabilities and limitations of a current Fortran implementation of the T-matrix method for randomly oriented, rotationally symmetric scatterers, *J. Quant. Spectrosc. Radiat. Transfer*, *60*, 309–324.

Perovich, D. K., and J. W. Govoni (1991), Absorption coefficients of ice from 250 to 400 nm, *Geophys. Res. Lett.*, *18*(7), 1233–1235.

Rapp, M., and G. E. Thomas (2006), Modeling the microphysics of mesospheric ice particles: Assessment of current capabilities and basic sensitivities, *J. Atmos. Sol. Terr. Phys.*, *68*(7), 715–744.

Rapp, M., G. E. Thomas, and G. Baumgarten (2007), Spectral properties of mesospheric ice clouds: Evidence for nonspherical particles, *J. Geophys. Res.*, *112*, D03211, doi:10.1029/2006JD007322.

Rusch, D. W., G. E. Thomas, and E. J. Jensen (1991), Particle size distributions in polar mesospheric clouds derived from Solar Mesosphere Explorer measurements, *J. Geophys. Res.*, *96*(D7), 12,933–12,939.

Siskind, D. E., M. E. Hervig, J. Gumbel, and M. H. Stevens (2007), Polar mesospheric cloud mass and the ice budget: 3. Application of a coupled ice-chemistry-dynamics model and comparison with observations, *J. Geophys. Res.*, *112*, D08303, doi:10.1029/2006JD007499.

Stevens, M. H., C. R. Englert, M. T. DeLand, and M. Hervig (2005), The polar mesospheric cloud mass in the Arctic summer, *J. Geophys. Res.*, *110*, A02306, doi:10.1029/2004JA010566.

Stevens, M. H., C. R. Englert, M. T. DeLand, and S. M. Bailey (2007), Polar mesospheric cloud mass and the ice budget: 2. Application to satellite data sets, *J. Geophys. Res.*, *112*, D08205, doi:10.1029/2006JD007532.

Taylor, M. J., M. Gadsden, R. P. Lowe, M. S. Zalcik, and J. Brausch (2002), Mesospheric cloud observations at unusually low latitudes, *J. Atmos. Sol. Terr. Phys.*, *64*, 991–999.

Thomas, G. E. (1984), Solar Mesosphere Explorer measurements of polar mesospheric clouds (noctilucent clouds), *J. Atmos. Terr. Phys.*, *46*(9), 819–824.

Thomas, G. E., and C. P. McKay (1985), On the particle size and water content of polar mesospheric clouds, *Planet. Space Sci.*, *33*(10), 1209–1224.

Thomas, G. E., R. D. McPeters, and E. J. Jensen (1991), Satellite observations of polar mesospheric clouds by the Solar Backscattered Ultraviolet spectral radiometer: Evidence of a solar cycle dependence, *J. Geophys. Res.*, *96*(D1), 927–939.

Turco, R. P., O. B. Toon, R. C. Whitten, R. G. Keesee, and D. Hollenbach (1982), Noctilucent clouds: Simulation studies of their genesis, properties and global influences, *Planet. Space Sci.*, *30*, 1147–1181.

von Cossart, G., J. Fiedler, and U. von Zahn (1999), Size distributions of NLC particles as determined from 3-color observations of NLC by ground-based lidar, *Geophys. Res. Lett.*, *26*(11), 1513–1516.

von Savigny, C., S. V. Petelina, B. Karlsson, E. J. Llewellyn, D. A. Degenstein, N. D. Lioyd, and J. P. Burrows (2005), Vertical variation of NLC particle sizes retrieved from Odin/OSIRIS limb scattering observations, *Geophys. Res. Lett.*, *32*, L07806, doi:10.1029/2004GL021982.

Warren, S. G. (1984), Optical constants of ice from the ultraviolet to the microwave, *Appl. Opt.*, *23*(8), 1206–1225.

Witt, G. (1962), Height, structure and displacement of noctilucent clouds, *Tellus*, *14*(1), 1–18.

Woods, T. N., et al. (1996), Validation of the UARS solar ultraviolet irradiances: Comparisons with the ATLAS 1 and 2 measurements, *J. Geophys. Res.*, *101*, 9541–9569.

C. R. Englert and M. H. Stevens, Space Science Division, Naval Research Laboratory, 4555 Overlook Avenue SW, Code 7641, Washington, DC 20375-5320, USA. (christoph.englert@nrl.navy. mil)